Conformations of Dimethoxydimethylsilane: Matrix Isolation Infrared and ab Initio Studies

V. Kavitha and K. S. Viswanathan*

Chemistry Group, Indira Gandhi Centre for Atomic Research, Kalpakkam 603 102 India

Received: October 18, 2006; In Final Form: December 26, 2006

Conformations of dimethoxydimethylsilane (DMDMS) were studied using matrix isolation infrared spectroscopy, by trapping the silane in argon and nitrogen matrixes. The matrix was deposited using both an effusive and a supersonic jet source. The effusive source was maintained at two different temperatures, viz. 298 and 433 K, during deposition to alter the conformational population of the silane. The experimental results were supported by computations performed at both the HF and B3LYP levels, using 6-31++G** basis set. Vibrational frequency calculations were carried out to assign the experimental features and also to ensure that the computed structures did indeed correspond to minima. A conformer with a $G^{\pm}G^{\mp}$ structure was found to be the ground state, while $G^{\pm}T$ and $G^{\pm}G^{\pm}$ structures were the next higher energy conformers with energies of 1.32 and 1.48 kcal/mol, respectively. Natural bond orbital analysis was carried out at both HF/6-31++G** and B3LYP/6-31++G** level which indicated that the charge-transfer hyperconjugative interactions largely determine the conformational preferences in this molecule. This interaction appears to be smaller in DMDMS than in the corresponding carbon analogue, dimethoxypropane (DMP).

Introduction

The reactivity and structural aspects of a number of important molecular systems, such as carbohydrates, acetals, and ketals, to name a few, are largely decided by the conformation about the C−O−C type linkage.[1,2] For example, in the case of sugars, the presence of the oxygen heteroatom in the ring, introduces the operation of the anomeric effect, which causes the axial form to be more stable. In contrast, in monoalkylcyclohexanes, the axial−equatorial equilibrium is favored toward the equatorial form, guided mainly by steric effects.[3−5] Dipole−dipole interactions or lone-pair repulsions have been considered as the origin of the anomeric effect. Salzner revisited the origin of the anomeric effect and concluded that anomeric effects are due to charge back-donation from lone pairs rather than dipole repulsions.[6] It can be explained as being due to the favorable overlap between the lone-pair orbital of oxygen with the antibonding σ^*_{CO} orbital. This favors the axial orientation of the substituent, which is evident from the fact that there is lengthening of the C−O bond. Crystallographic data also support the existence of these effects.[2] The anomeric effect is well recognized as an important factor in defining the predominant conformational state of many cyclic heteroatom-containing compounds.[7−12] The geometry of the conformations of the transition state or of the intermediate establishes the selectivity of the chemical reactions and the stereochemistry of adducts.[13−18] In recent years, an increasing number of investigations have been concerned with the anomeric effect and the conformational analysis of tetrahydropyrans, glycosides and other cyclohexane derivatives.[3,4,5,17,19−28]

In recent times, we have studied the structural aspects of a number of acetals and ketals, such as dimethoxymethane, 1,1-dimethoxyethane, and dimethoxypropane.[29−31] These compounds have served for us as model compounds to eventually understand the role of anomeric effects on the conformational preferences in alkyl phosphates. The alkyl phosphates, themselves, are industrially important; they are the solvents of choice in many solvent extraction processes and are also used as pesticides, etc. A fundamental understanding of these processes requires a thorough study of the structural aspects of the phosphates.

In a study of the acetals and ketals referred to above, we have been interested on the magnitude of the anomeric effects, in corresponding silicon systems and we had reported our work on a few related silicon systems, such as trimethoxymethylsilane[32] and dimethoxymethylsilane.[33] These silicon systems themselves are quite important as they are used as coupling reagents, cross-linkers, and adhesion promoting primers. However, the data on the conformations of these compounds are sparse. Conformations of these molecules need to be studied for a better understanding of their reaction kinetics.

In the series of the silicon compounds, DMDMS provides a good case for the operation of anomeric effects in silicon compounds. A few studies exist in the literature on this molecule. Winkler et al.[34] have studied DMDMS using electron impact energy loss spectroscopy near the Si 2p ionization edge. The substituent effects on LUMO energies and NMR shieldings were considered in this study, which also used ab initio computations to calculate the structure of the silicon compounds. No details of the ground state geometry were given, except that a C_{2v} structure was considered as the ground state conformer. Tajima et al.[35] have studied DMDMS by mass-analyzed ion kinetic energy (MIKE) spectrometry. They concluded that the fragmentation pattern for silicon compounds is similar to that of the carbon analogues, thought the mechanism of fragmentation is likely different in the two systems. Using X-ray absorption near-edge spectroscopy, Sutherland et al.[36] studied DMDMS with the objective of using the gas-phase spectra as analogs for the Si 2p spectra of the solid-state compounds. Maier et al.[37] synthesized DMDMS, in situ, in an argon matrix by the reacting silicon atoms with dimethylether and studied the mechanism of these reactions. On the basis of ab initio computations performed at the B3LYP/6-311+G** level the vibrational features were assigned to $G^{\pm}G^{\mp}$ conformer. Ignatyev

* Corresponding author: E-mail: vish@igcar.gov.in.

10.1021/jp066837j CCC: $37.00
Published on Web 02/22/2007

et al.[38] studied the structure of a series of methoxysilanes and their hydrolysis product using vibrational spectroscopy. However, information regarding the higher energy conformers was not presented. In this paper, we present the results of our study on the ground and higher energy conformations of DMDMS.

Experimental Section

Matrix isolation experiments were carried out using a Leybold AG helium-compressor-cooled closed cycle cryostat. The details of the vacuum system and experimental setup are described elsewhere.[39−41] The typical sample to matrix ratio in all our experiments was 1:1000. The sample and the matrix gas were mixed in a mixing chamber, streamed out of a single jet nozzle, and deposited onto a cold KBr substrate maintained at ∼12 K. Deposition was carried out at the rate of ∼3 mmol/h and a typical deposition lasted for ∼1 h. The spectra were recorded using a BOMEM MB 100 FTIR spectrometer with a spectral resolution of 1 cm^{-1}. After a spectrum was recorded, the matrix was warmed to 35 K, kept at this temperature for 15 min and recooled to ∼12 K. The spectra of the matrix thus annealed were recorded. Experiments were carried out by maintaining the effusive source at two different nozzle temperatures, viz. 298 and 433 K. In the hot nozzle experiments, the nozzle was heated to 433 K, over a length of 35 mm, just prior to the exit of the gas mixture. We also performed a few experiments using a pulsed supersonic jet source (Parker Hannifin Corporation), with a pulse width of 2 ms and a repetition rate of 0.5 Hz, to deposit the matrix. A stagnant pressure of typically 1.3 atm was used in these experiments. At this deposition rate, the temperature of the cryotip did not rise.

Dimethoxydimethylsilane (97%, Lancaster) was used without any further purification. However, the sample was subjected to several freeze−pump−thaw cycles before performing the experiments.

Computational Details

Computations were carried out using the Gaussian suite of program G98W on a Pentium IV machine.[42] All the structures were optimized without imposing any symmetry constraints during optimization process. Structure optimizations were carried out at both HF and B3LYP levels using a 6-31++G** basis set. Vibrational frequency calculations were performed at both the levels of theory using analytical gradients; first, to ensure that the computed structures did correspond to minima on the potential surface and also to assign the vibrational features observed in the experiments. The computed vibrational frequencies, at the B3LYP/6-31++G** level, were scaled to bring them in agreement with the experimental vibrational frequencies. To arrive at the scaling factor the experimentally observed strongest feature (1086.8 cm^{-1}) was correlated with the strongest computed feature for the ground state conformer. The scaling factor that brought the computed frequency in agreement with the experimentally observed frequency was used to scale all the other vibrational frequencies. The scaling factor turned out to be 0.9826 for the vibrational frequencies calculated at the B3LYP/6-31++G** level. The computed frequencies were used to simulate a vibrational spectra using SYNSPEC program.[43] The structure and energy of the transition state connecting the ground state and first higher energy conformer was also computed. To understand the nature of the orbital interactions in determining conformational preferences, Natural bond orbital (NBO) (Version 3.1) analysis, invoked through Gaussian G98W, were performed at HF and B3LYP levels of theory, using the 6-31++G** basis set. The use of NBO has been shown to provide a detailed understanding of conformational preferences in several such systems.[44−49] To ascertain the role of orbital interactions, we also performed calculations, where specific orbitals were deleted from the function space, using the NBODEL option.

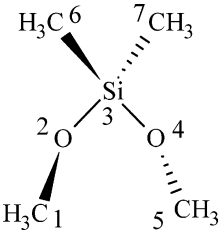

Figure 1. Structure of DMDMS showing atom numbering.

The notations used to denote the conformers of DMDMS, which arise due to the rotation of the terminal carbon atom about the Si−O bond, are discussed here. If the terminal carbon atom C1 is oriented gauche with respect to O4 (Figure 1), it is denoted by a "G" , and if oriented anti, it is denoted by a "T" . Furthermore, in the conformations with gauche orientations, if both C1 and C5 are oriented on the same side of the O2−Si3-O4 plane, they are denoted by the same superscript sign, i.e., G^+G^+ or G^-G^-; if they are oriented on opposite sides of the reference plane, they are denoted by G^+G^- or G^-G^+. In a molecule such as dimethoxysilane (DMS), the symmetry of the molecule renders the pair G^+G^- and G^-G^+, degenerate and hence can be grouped together and denoted as $G^{\pm}G^{\mp}$. Likewise, the pair of conformers $G^{\pm}G^{\pm}$ are also degenerate. This degeneracy is however lifted for dimethoxymethylsilane (DMMS), due to the presence of methyl group on the Si atom, which makes the two sides of the reference plane (O2−Si3−O4 plane) nonequivalent.[33] In the case of the DMDMS, the presence of two methyl groups, one on each side of the reference plane, again renders the molecule symmetric, and hence the pairs of conformers referred to above are again degenerate, as in DMS, and are grouped together. This notation is identical to that we used in our studies on DME and DMMS.[30,33]

Results and Discussions

Experimental Details. Figure 2 shows the matrix isolation infrared spectra of DMDMS trapped in argon. The spectra span the region 1300−1050 cm^{-1} (grid A) and 910−760 cm^{-1} (grid B), which correspond to $O-CH_3$ stretching and CH_3 rocking vibrations. Also shown in Figure 2, traces b and c, are the matrix isolated infrared spectra of DMDMS trapped in argon using hot nozzle effusive source (433 K) and supersonic nozzle respectively.

The main spectral features of DMDMS occur at 804.7, 848.6, 864.5, 1086.8, 1106.5, 1192.8, 1257.9, and 1263. 2 cm^{-1}. In the spectra recorded with a supersonic jet source, there are minor changes, such as the reduction in the intensities of the 1106 cm^{-1} feature. The same feature also appear to be somewhat enhanced in the spectra recorded with effusive nozzle maintained at an elevated temperature of 433 K (Figure 2).

When the matrix was annealed at 35 K, no perceptible changes in the features were observed; hence only the spectra obtained in preannealed matrixes are presented and discussed. We also recorded the spectra of DMDMS in a nitrogen matrix. The spectral features observed in the nitrogen matrix were generally similar to that observed in the Ar matrix, with the features in the N_2 matrix being slightly shifted from argon matrix values.

Computations. We performed geometry optimizations at HF and B3LYP levels of theory using 6-31++G** basis set. At

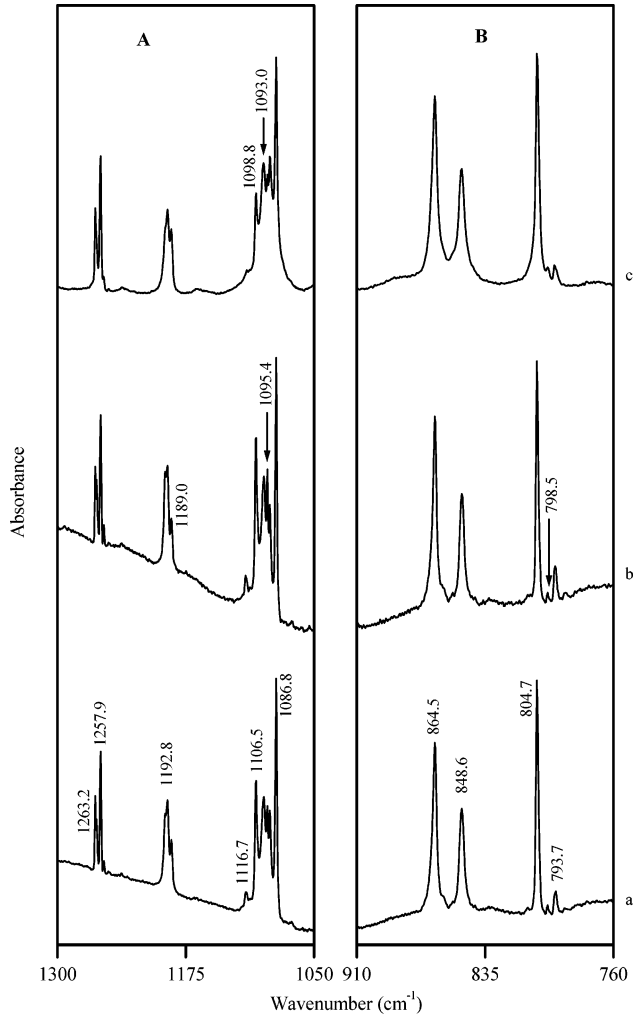

Figure 2. Matrix isolation infrared spectra of DMDMS trapped in argon spanning the region 1300−1050 cm^{-1} (grid A) and 910−760 cm^{-1} (grid B). IR spectra of DMDMS deposited using (a) a room-temperature effusive source, (b) an effusive source at 433 K, and (c) a supersonic nozzle. The spectra shown here are those recorded in preannealed matrixes.

both the levels of theory, four nonequivalent-by-symmetry minima corresponding to conformers with $G^{\pm}G^{\mp}$, $G^{\pm}T$, $G^{\pm}G^{\pm}$ and TT structures were obtained.

Selected molecular parameters of the four conformers optimized at the B3LYP/6-31++G** level, are given in Table 1. (To avoid repetitive reproduction of data, only the B3LYP computed parameters are given in the table.) The corresponding structures are shown in Figure 3, together with the relative energies of the conformers with respect to the ground state conformer. As can be seen from Table 1, both Si3−O2 and Si3−O4 bond lengths are longer in $G^{\pm}G^{\mp}$ conformer compared with the corresponding bond lengths in the TT conformer, where no anomeric effect operates. The fact that both Si3−O2 and Si3−O4 bonds are equal in the $G^{\pm}G^{\mp}$ conformer, indicates that the anomeric effect operates such as to involve the electrons on both O2 and O4 and both the Si−O bonds. However, in the $G^{\pm}T$ conformer the Si3−O4 bond is longer compared to Si3−O2 bond implying that anomeric effect operates only in that part of the molecule, involving the nonbonded electrons on oxygen, O2.

The relative energies of the conformers of DMDMS corrected for ZPE at the HF and B3LYP levels of theory are given in Table 2. Also given in this table are the energies of the transition states connecting the various minima.

TABLE 1: Selected Optimized Parameters[a] of the Conformers of DMDMS Computed at the B3LYP/ 6-31++G Level**

parameter	$G^{\pm}G^{\mp}$	$G^{\pm}T$	$G^{\pm}G^{\pm}$	TT
O2−C1	1.4228	1.4227	1.4183	1.4178
Si3−O2	1.6729	1.6605	1.6710	1.6635
O4−Si3	1.6724	1.6746	1.6705	1.6630
C5−O4	1.4224	1.4185	1.4183	1.4178
C6−Si3	1.8734	1.8827	1.8641	1.8816
C7−Si3	1.8730	1.8714	1.8851	1.8816
Si3−O2-C1	124.29	125.24	127.85	125.94
O4−Si3-O2	110.44	105.75	111.97	102.27
C5−O4-Si3	124.85	125.85	126.96	126.17
C6−Si3-O4	104.27	109.52	105.43	110.92
C7−Si3-O4	112.05	111.71	109.58	110.75
O4−Si3-O2−C1	**58.90**	**52.44**	**−81.56**	**−167.52**
C5−O4-Si3−O2	**61.76**	**−173.67**	**65.34**	**−166.44**

[a] Bond distances in Å; bond angles and torsion angles in degrees. Torsional angles of the fragment ABCD denote the angle between ABC and BCD planes.

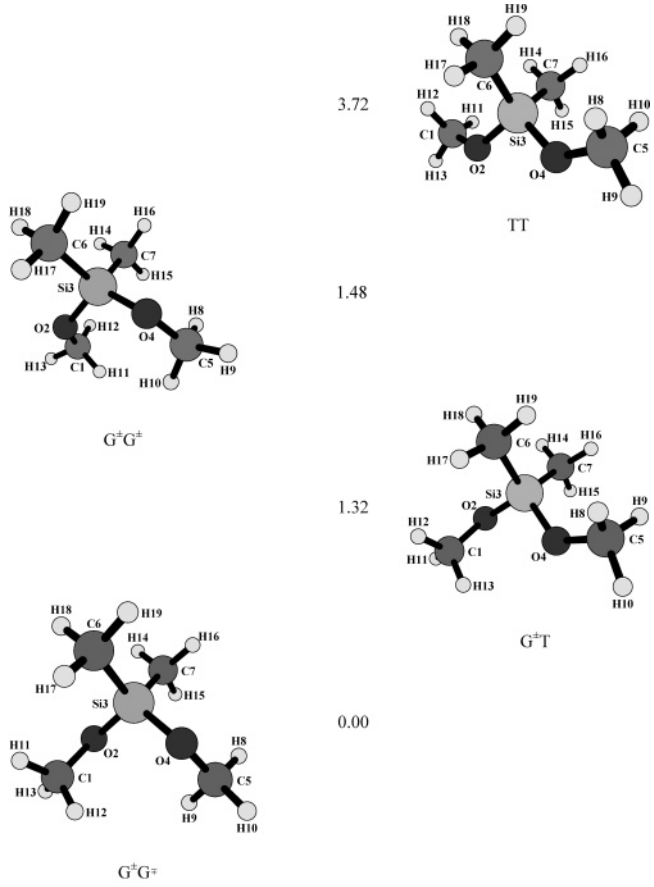

Figure 3. Structure of the conformers of DMDMS. Relative energies of the conformers with respect to the ground state conformer are given against each structure.

Vibrational Assignments. The spectral features at 804.7, 848.7, 1086.9, 1095.5, 1189.0, 1192.9, 1258.0, and 1263.2 cm^{-1} obtained when DMDMS was trapped in argon, agree well with the B3LYP/6-31++G** computed scaled frequencies of the ground state conformer, $G^{\pm}G^{\mp}$, and hence only the B3LYP computed frequencies have been considered in this discussion. The vibrational mode assignments are given in Table 3.

It can be seen from Table 2 that the conformers with $G^{\pm}T$ and $G^{\pm}G^{\pm}$ structures occur at about ∼1.3 kcal/mol above the ground state conformer. At room temperature the ratio of the population of the conformers $G^{\pm}G^{\mp}$, $G^{\pm}T$ and $G^{\pm}G^{\pm}$ would be 0.77:0.17:0.06 and hence the contributions of $G^{\pm}T$ and $G^{\pm}G^{\pm}$

TABLE 2: Zero Point Vibrational Energies (hartree/Particle), Relative Energies (kcal/mol) and Dipole Moments (debye), of the Conformers of DMDMS Computed at HF and B3LYP Level Using 6-31++G Basis Set, Where Degeneracies of the Conformers Are Given in Parentheses**

	zero point energy (hartree/particle)		relative energy (ZPE corrected) (kcal/mol)		dipole moment (debye)	
conformer	HF[a]	B3LYP[b]	HF	B3LYP	HF	B3LYP
$G^{\pm}G^{\mp}(2)$	0.147112	0.156150	0.00[c]	0.00[d]	0.56	0.40
$G^{\pm}T(4)$	0.146921	0.156128	1.11	1.32	2.02	1.70
$G^{\pm}G^{\pm}(2)$	0.146969	0.156232	1.56	1.48	2.10	2.10
TT(1)	0.146718	0.155851	3.58	3.72	2.19	2.22
TS[e]		0.155999		1.76		1.13
TS[f]		0.156097		1.71		2.05
TS[g]		0.156073		2.06		1.48

[a] Scaling factor 0.8694. [b] Scaling factor 0.9826. [c] Energy of the ground state conformer without ZPE correction −597.2242419 hartrees at the HF level. [d] Energy of the ground state conformer without ZPE correction −599.7168179 hartrees at the B3LYP level. [e] Transition state connecting $G^{\pm}G^{\mp}$ and $G^{\pm}T$. [f] Transition state connecting $G^{\pm}T$ and $G^{\pm}G^{\pm}$. [g] Transition state connecting $G^{\pm}G^{\mp}$ and $G^{\pm}G^{\pm}$.

conformers to the room-temperature effusive source spectra cannot be ruled out. To rationalize this observation, we carried out a few experiments using hot nozzle source, where the nozzle temperatures were varied from room temperature (∼300 K) to 433 K. These experiments were performed in an effort to alter the ratio of the population of the conformers just prior to deposition. At 433 K, the population ratio of the three conformers was calculated to be 0.62:0.27:0.11; a marginal change from the room-temperature ratio. We also performed experiments with a supersonic nozzle source to look for conformational cooling. As a result of the expansion, one would expect a decrease in the intensity of the spectral features corresponding to the higher energy conformer. While minor changes in the spectra recorded under the different experimental conditions were observed, it was difficult to attribute these small changes unambiguously to the presence of higher energy conformers, as the vibrational features of the ground state and higher energy conformers occur not well resolved from each other.

We also computed the transition state structure connecting the ground state and the higher energy conformers. Vibrational frequency calculations showed that the structures were first-order saddle points and that the magnitude of the single imaginary frequency for each saddle point was between −60 and −80 cm^{-1}. Intrinsic reaction coordinate calculations were performed to confirm that the transition structures did indeed connect the minima in question. The barrier for interconversion from the $G^{\pm}T$ conformer to the ground state conformer was calculated to be 0.44 kcal/mol while the barrier for interconversion from the $G^{\pm}G^{\pm}$ to the ground state was computed to be 0.58 kcal/mol. It can be argued that the barrier being as small they are, the higher energy conformers, can likely interconvert to the ground state conformer during deposition.[50] It is only a matter of speculation, as to how the barrier mentioned above, which is a free molecule barrier, would be altered in the matrix. As a result of the small barrier, coupled with the fact that the features of the ground and higher energy conformers occur not well resolved from each other, we will refrain from assigning any of the changes in the spectra to higher energy conformers. More work is clearly necessary to firmly identify the presence, or not, of higher energy conformers. The small changes in spectral features observed when the matrix was deposited using a hot nozzle source and a supersonic source may be alternately explained as site-split features of the ground state conformer.

Figure 4 shows a comparison of the matrix isolated infrared spectra with the computed spectra of the ground state conformer of DMDMS. It can be seen that the computed spectrum agrees well with the experimental spectrum, indicating that the observed features are mainly due to the ground state conformer.

TABLE 3: Experimental Vibrational Frequencies in Argon and Nitrogen Matrixes and Computed Scaled Frequencies[a] of $G^{\pm}G^{\mp}$, $G^{\pm}T$ and $G^{\pm}G^{\pm}$ Conformers of DMDMS Computed at the B3LYP/6-31++G Level, Where Intensities[b] are Given in Parenthesis**

	computational			experimental	
mode assignments[c]	$G^{\pm}G^{\mp}$	$G^{\pm}T$	$G^{\pm}G^{\pm}$	argon	nitrogen
C−O−Si deform + Si−CH_3 rock	713.8(38)	713.3(34)	711.1(37)		
	717.8(32)	724.5(38)	712.1(39)		
Si−CH_3 rock	800.6(127)	792.3(132)	800.7(125)	804.7, 793.7	795.4, 798.4, 804.7
	860.8(114)	859.0(138)	858.3(111)	848.6	848.6
	866.0(176)			864.5	864.0
		866.9(142)	860.4(174)		
SiO−CH_3 stretch	1086.8(280)			1086.8, 1098.8	1084.4, 1091.1
		1098.0(390)	1100.1(204)		
	1095.4(233)			1095.4, 1106.5, 1116.9	1095.4, 1098.3, 1101.7, 1110.5
		1108.7(146)	1116.6(286)		
OCH_3 rock	1182.6(52)			1189.0	1190.0
		1185.8(74)	1186.1(59)		
	1184.4(49)			1192.8, 1195.2	1192.4
		1187.2(41)	1189.6(74)		
Si−CH_3 sym deform	1280.9(55)			1257.9, 1254.6	1258.5, 1259.9
		1279.5(54)	1281.2(51)		
	1285.1(35)			1263. 2, 1261.9	1262.8, 1264.7
		1283.0(38)	1285.3(38)		
OCH_3 sym stretch	2956.7(91)	2948.7(80)	2954.6(119)	no firm assignments made	
	2957.8(55)	2959.4(72)			
OCH_3 asym stretch	3014.5(45)	3003.2(52)	3010.8(88)		
	3016.2(47)	3024.5(43)			
	3053.5(58)	3050.7(41)	3047.9(69)		

[a] Scaling factor 0.9826. [b] Intensities are given in km/mol. [c] Mode assignments were made using the vibrational visualization program Gauss view 2.1.

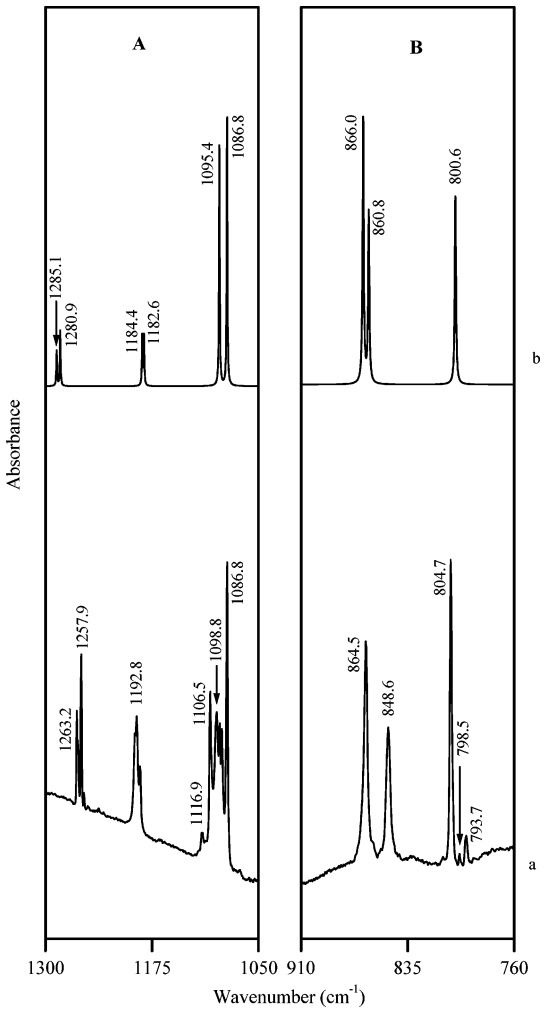

Figure 4. Comparison of the experimental and computed spectra of DMDMS. The spectra span the region 1300−1050 cm^{-1} (grid A) and 910−760 cm^{-1} (grid B). (a) Matrix isolation infrared spectra of DMDMS recorded using room-temperature effusive source. (b) Computed spectra of $G^{\pm}G^{\mp}$ conformer.

NBO Analysis. NBO analysis was performed to understand the role of hyperconjugative interactions toward conformational preferences in DMDMS. The energies associated with the charge transfer interactions are obtained from the second-order perturbation estimates of the Fock matrix in the NBO basis and are shown in Table 4. The analysis reveals that the strongest stabilization stems from the interaction of a filled nonbonded orbital on oxygen with an empty antibonding orbital of Si−O. More specifically, in the ground state conformer, $G^{\pm}G^{\mp}$, the strongest charge transfer interactions involve the donor lone pair on oxygen, O2 with acceptor, σ^*_{Si3-O4}, and the donor lone pair on O4 with σ^*_{Si3-O2}. As shown in Table 4, there are other hyperconjugative interactions of these lone pairs with antibonding orbitals, such as σ^*_{C1-H11}, σ^*_{C1-H12}, σ^*_{Si3-C6}, σ^*_{Si3-C7}, σ^*_{C5-H8}, σ^*_{C5-H9}, which, however, are weaker than those involving the σ^*_{Si3-O4} and σ^*_{Si3-O2}. A comparison of these delocalization interactions in the higher energy conformer, $G^{\pm}T$ is interesting. The strongest delocalization interaction in this conformer, again involves the lone pair on O2 with the antibonding σ^*_{Si3-O4} orbital; however, the magnitude of the interaction in the $G^{\pm}T$ conformer is less than that in the $G^{\pm}G^{\mp}$ conformer. Furthermore, there is no corresponding strong interaction involving the lone pair on the O4 oxygen and the corresponding σ^*_{Si3-O2}, as was seen with the $G^{\pm}G^{\mp}$ conformer. In the $G^{\pm}G^{\pm}$ conformer, it can be seen that the charge transfer interactions involving the nonbonded electrons on both oxygens, O2 and O4, with the σ^*_{Si3-O4} and σ^*_{Si3-O2}, respectively, are once again observed, as in the ground state $G^{\pm}G^{\mp}$ conformer. However, in spite of the charge transfer interactions being comparable in the $G^{\pm}G^{\mp}$ and $G^{\pm}G^{\pm}$ conformers, the latter turns out to be a higher energy structure, most likely due to steric reasons. In the $G^{\pm}G^{\pm}$ structure, three of the methyl groups, two terminal and one on the central Si atom, are oriented on the same side, leading to a steric crowding. In the TT conformer, no charge delocalization interactions are indicated.

An examination of the occupancies of the various orbitals involved in the hyperconjugative interactions is also interesting (Table 5). In the ground state $G^{\pm}G^{\mp}$ conformer of DMDMS, the occupancy of the lone pair on the oxygen involved in the delocalization is reduced relative to the lone pair not participating in the hyperconjugation by about 0.0438e. This reduction in occupancy is approximately equal for the both the oxygens, O2 and O4, as the anomeric stabilization operates on both the oxygens. However, in the higher energy $G^{\pm}T$ conformer, it can be seen, that the reduction in occupancy on the lone pair of oxygen, O2, participating in the delocalization, is greater than for the lone pair orbitals on O4, as the anomeric stabilization is absent in this part of the molecule. Likewise, both σ^*_{Si3-O2} and σ^*_{Si3-O4} acceptor orbitals show significant and nearly equal occupancies (0.0849e) in the $G^{\pm}G^{\mp}$ conformer, while the σ^*_{Si3-O4} acceptor orbitals shows greater occupancy (0.0798e) in the $G^{\pm}T$ conformer relative to the σ^*_{Si3-O2} orbital, indicating the absence of the $n_{O4}-\sigma^*_{Si3-O2}$ interaction. The occupancies of the $G^{\pm}G^{\pm}$ conformers mimic the behavior of the ground state $G^{\pm}G^{\mp}$ conformer, indicating that this conformer enjoys about the same charge delocalization interaction as the ground state conformer.

Comparison of the Conformational Picture in DMDMS and DMP. It is instructive to compare the conformational preferences in the two related molecules, DMDMS and its carbon analogue, DMP. In both these systems, the $G^{\pm}G^{\mp}$ conformer is the ground state structure, with the $G^{\pm}T$ structure being the first higher energy conformer. While the energy difference between these two structures, at the B3LYP/6-31++G** level, was only 1.32 kcal/mol in the case of DMDMS (Table 2), it was 3.25 kcal/mol for DMP, indicating that the factors favoring the ground state in DMP probably have a greater influence than they do in DMDMS; in other words, the hyperconjugative interactions in DMP are likely stronger than in DMDMS.[31]

To estimate, in a more quantitative sense, the relative contributions of these interactions, in deciding conformational preferences in DMDMS and DMP, we studied the effect of deleting the acceptor orbitals on the energies of the ground state and the first higher energy structures. Table 6 gives the energies of the $G^{\pm}G^{\mp}$ and $G^{\pm}T$ conformers in DMDMS and DMP, after deleting the various acceptor orbitals or combinations of acceptor orbitals, which participated strongly in the hyperconjugative interactions described earlier. These computations involving the deletion of specific orbital were performed at the HF/6-31++G** level.

While both acceptor orbitals, σ^*_{Si3-O2} and σ^*_{Si3-O4}, affect the energy of the $G^{\pm}G^{\mp}$ conformer in DMDMS, the orbital σ^*_{Si3-O2} has a smaller influence on the $G^{\pm}T$ structure, as it is not a strongly participating acceptor in this conformer. The same trend is also seen in the DMP molecule. Interestingly, while deleting the σ^*_{Si3-O2} and σ^*_{Si3-O4} acceptor orbital in the $G^{\pm}G^{\mp}$ conformer of DMDMS increased the energy by about 0.019%, the same exercise (i.e., deleting the corresponding σ^*_{C3-O2} and

TABLE 4: Energies (kcal/mol), Difference in Energies of Acceptor and Donor Orbitals (Hartrees) and Fock Matrix Elements (Hartrees) for $G^{\pm}G^{\mp}$, $G^{\pm}T$, $G^{\pm}G^{\pm}$, and TT Conformers of DMDMS and DMP Calculated at the B3LYP/6-31++G Level**

$G^{\pm}G^{\mp}$

DMDMS					DMP				
Donor orbital	Acceptor orbital	E_2 (kcal/mol)	E_j-E_i (Hartrees)	F(i,j) (Hartrees)	Donor orbital	Acceptor orbital	E_2 (kcal/mol)	E_j-E_i (Hartrees)	F(i,j) (Hartrees)
n^1_{O4}	$\sigma^*_{O2\text{-}Si3}$	1.06	0.76	0.026	n^1_{O4}	$\sigma^*_{O2\text{-}C3}$	1.02	0.84	0.026
n^1_{O2}	$\sigma^*_{Si3\text{-}O4}$	1.22	0.76	0.027	n^1_{O2}	$\sigma^*_{C3\text{-}O4}$	0.94	0.84	0.025
n^2_{O2}	$\sigma^*_{C1\text{-}H11}$	5.74	0.74	0.059	n^2_{O2}	$\sigma^*_{C1\text{-}H11}$	6.25	0.73	0.062
n^2_{O2}	$\sigma^*_{C1\text{-}H12}$	5.23	0.74	0.057	n^2_{O2}	$\sigma^*_{C1\text{-}H12}$	4.67	0.74	0.053
n^2_{O2}	$\sigma^*_{Si3\text{-}O4}$	9.34	0.57	0.065	n^2_{O2}	$\sigma^*_{C3\text{-}O4}$	13.67	0.58	0.080
n^2_{O2}	$\sigma^*_{Si3\text{-}C6}$	5.17	0.58	0.049	n^2_{O2}	$\sigma^*_{C3\text{-}C6}$	4.31	0.66	0.048
n^2_{O4}	$\sigma^*_{O2\text{-}Si3}$	9.68	0.57	0.066	n^2_{O4}	$\sigma^*_{O2\text{-}C3}$	13.35	0.58	0.079
n^2_{O4}	$\sigma^*_{Si3\text{-}C7}$	4.91	0.58	0.048	n^2_{O4}	$\sigma^*_{C3\text{-}C7}$	4.43	0.66	0.049
n^2_{O4}	$\sigma^*_{C5\text{-}H8}$	5.75	0.74	0.059	n^2_{O4}	$\sigma^*_{C5\text{-}H8}$	6.22	0.73	0.061
n^2_{O4}	$\sigma^*_{C5\text{-}H9}$	5.23	0.74	0.057	n^2_{O4}	$\sigma^*_{C5\text{-}H10}$	6.22	0.73	0.061

$G^{\pm}T$

DMDMS					DMP				
Donor orbital	Acceptor orbital	E_2 (kcal/mol)	E_j-E_i (Hartrees)	F(i,j) (Hartrees)	Donor orbital	Acceptor orbital	E_2 (kcal/mol)	E_j-E_i (Hartrees)	F(i,j) (Hartrees)
n^1_{O4}	$\sigma^*_{O2\text{-}Si3}$	4.39	0.76	0.052	n^1_{O4}	$\sigma^*_{O2\text{-}C3}$	3.96	0.85	0.052
n^1_{O2}	$\sigma^*_{Si3\text{-}O4}$	1.60	0.75	0.031	n^1_{O2}	$\sigma^*_{C3\text{-}O4}$	0.93	0.82	0.025
n^2_{O2}	$\sigma^*_{C1\text{-}H12}$	5.30	0.74	0.057	n^2_{O2}	$\sigma^*_{C1\text{-}H11}$	5.90	0.73	0.060
n^2_{O2}	$\sigma^*_{C1\text{-}H13}$	5.43	0.75	0.058	n^2_{O2}	$\sigma^*_{C1\text{-}H12}$	5.04	0.75	0.056
n^2_{O2}	$\sigma^*_{Si3\text{-}O4}$	7.54	0.56	0.058	n^2_{O2}	$\sigma^*_{C3\text{-}O4}$	12.50	0.57	0.076
n^2_{O2}	$\sigma^*_{Si3\text{-}C6}$	6.29	0.57	0.054	n^2_{O2}	$\sigma^*_{C3\text{-}C6}$	5.16	0.64	0.052
n^2_{O4}	$\sigma^*_{O2\text{-}Si3}$	-	-	-	n^2_{O4}	$\sigma^*_{O2\text{-}C3}$	1.05	0.61	0.023
n^2_{O4}	$\sigma^*_{Si3\text{-}C7}$	7.54	0.58	0.060	n^2_{O4}	$\sigma^*_{C3\text{-}C7}$	7.15	0.67	0.062
n^2_{O4}	$\sigma^*_{C5\text{-}H8}$	4.81	0.73	0.054	n^2_{O4}	$\sigma^*_{C5\text{-}H8}$	5.45	0.73	0.057
n^2_{O4}	$\sigma^*_{C5\text{-}H9}$	6.46	0.73	0.062	n^2_{O4}	$\sigma^*_{C5\text{-}H10}$	6.45	0.73	0.062

$G^{\pm}G^{\pm}$

DMDMS					DMP				
Donor orbital	Acceptor orbital	E_2 (kcal/mol)	E_j-E_i (Hartrees)	F(i,j) (Hartrees)	Donor orbital	Acceptor orbital	E_2 (kcal/mol)	E_j-E_i (Hartrees)	F(i,j) (Hartrees)
n^1_{O4}	$\sigma^*_{O2\text{-}Si3}$	0.93	0.75	0.024	n^1_{O4}	$\sigma^*_{O2\text{-}C3}$	-	-	-
n^1_{O2}	$\sigma^*_{Si3\text{-}O4}$	-	-	-	n^1_{O2}	$\sigma^*_{C3\text{-}O4}$	2.07	0.83	0.037
n^2_{O2}	$\sigma^*_{C1\text{-}H11}$	7.01	0.74	0.065	n^2_{O2}	$\sigma^*_{C1\text{-}H11}$	6.41	0.74	0.062
n^2_{O2}	$\sigma^*_{C1\text{-}H12}$	3.23	0.73	0.044	n^2_{O2}	$\sigma^*_{C1\text{-}H12}$	5.05	0.72	0.055
n^2_{O2}	$\sigma^*_{Si3\text{-}O4}$	11.17	0.57	0.072	n^2_{O2}	$\sigma^*_{C3\text{-}O4}$	10.68	0.58	0.070
n^2_{O2}	$\sigma^*_{Si3\text{-}C6}$	0.89	0.021	0.59	n^2_{O2}	$\sigma^*_{C3\text{-}C7}$	5.55	0.64	0.054
n^2_{O4}	$\sigma^*_{O2\text{-}Si3}$	9.89	0.57	0.067	n^2_{O4}	$\sigma^*_{O2\text{-}C3}$	14.85	0.58	0.083
n^2_{O4}	$\sigma^*_{Si3\text{-}C7}$	4.55	0.58	0.046	n^2_{O4}	$\sigma^*_{C3\text{-}C7}$	1.06	0.65	0.024
n^2_{O4}	$\sigma^*_{C5\text{-}H8}$	3.06	0.73	0.043	n^2_{O4}	$\sigma^*_{C5\text{-}H8}$	6.34	0.73	0.062
n^2_{O4}	$\sigma^*_{C5\text{-}H10}$	7.01	0.74	0.066	n^2_{O4}	$\sigma^*_{C5\text{-}H10}$	5.44	0.72	0.057

TT

DMDMS					DMP				
Donor orbital	Acceptor orbital	E_2 (kcal/mol)	E_j-E_i (Hartrees)	F(i,j) (Hartrees)	Donor orbital	Acceptor orbital	E_2 (kcal/mol)	E_j-E_i (Hartrees)	F(i,j) (Hartrees)
n^1_{O4}	$\sigma^*_{O2\text{-}Si3}$	3.95	0.75	0.049	n^1_{O4}	$\sigma^*_{O2\text{-}C3}$	4.24	0.83	0.053
n^1_{O2}	$\sigma^*_{Si3\text{-}O4}$	3.97	0.75	0.049	n^1_{O2}	$\sigma^*_{C3\text{-}O4}$	4.24	0.83	0.053
n^2_{O2}	$\sigma^*_{C1\text{-}H11}$	4.79	0.73	0.054	n^2_{O2}	$\sigma^*_{C1\text{-}H11}$	5.69	0.73	0.058
n^2_{O2}	$\sigma^*_{C1\text{-}H12}$	6.54	0.73	0.063	n^2_{O2}	$\sigma^*_{C1\text{-}H12}$	6.41	0.73	0.062
n^2_{O2}	$\sigma^*_{Si3\text{-}O4}$	0.75	0.57	0.019	n^2_{O2}	$\sigma^*_{C3\text{-}O4}$	1.36	0.59	0.025
n^2_{O2}	$\sigma^*_{Si3\text{-}C6}$	7.96	0.57	0.061	n^2_{O2}	$\sigma^*_{C3\text{-}C6}$	7.65	0.65	0.063
n^2_{O4}	$\sigma^*_{O2\text{-}Si3}$	0.86	0.57	0.020	n^2_{O4}	$\sigma^*_{O2\text{-}C3}$	1.36	0.59	0.025
n^2_{O4}	$\sigma^*_{Si3\text{-}C7}$	8.00	0.58	0.061	n^2_{O4}	$\sigma^*_{C3\text{-}C7}$	7.65	0.65	0.063
n^2_{O4}	$\sigma^*_{C5\text{-}H8}$	4.29	0.73	0.051	n^2_{O4}	$\sigma^*_{C5\text{-}H8}$	5.71	0.73	0.058
n^2_{O4}	$\sigma^*_{C5\text{-}H10}$	6.82	0.73	0.064	n^2_{O4}	$\sigma^*_{C5\text{-}H10}$	6.40	0.73	0.062

TABLE 5: Electron Occupancies of the Various NBOs in the $G^{\pm}G^{\mp}$, $G^{\pm}T$, $G^{\pm}G^{\pm}$ and TT Conformers of DMDMS and DMP Computed at the B3LYP/6-31++G Level**

DMDMS			DMP		
conformer	NBO	occupancy	conformer	NBO	occupancy
$G^{\pm}G^{\mp}$	n^1_{O2}	1.948 10	$G^{\pm}G^{\mp}$	n^1_{O2}	1.963 61
	n^2_{O2}	1.904 35		n^2_{O2}	1.907 68
	n^1_{O4}	1.947 86		n^1_{O4}	1.963 65
	n^2_{O4}	1.904 11		n^2_{O4}	1.908 45
	σ^*_{O2-Si3}	0.084 94		σ^*_{O2-C3}	0.076 57
	σ^*_{Si3-O4}	0.084 47		σ^*_{C3-O4}	0.077 27
$G^{\pm}T$	n^1_{O2}	1.946 29	$G^{\pm}T$	n^1_{O2}	1.961 36
	n^2_{O2}	1.907 04		n^2_{O2}	1.910 16
	n^1_{O4}	1.943 36		n^1_{O4}	1.952 74
	n^2_{O4}	1.912 71		n^2_{O4}	1.925 07
	σ^*_{O2-Si3}	0.058 45		σ^*_{O2-C3}	0.054 38
	σ^*_{Si3-O4}	0.079 82		σ^*_{C3-O4}	0.075 70
$G^{\pm}G^{\pm}$	n^1_{O2}	1.945 36	$G^{\pm}G^{\pm}$	n^1_{O2}	1.959 47
	n^2_{O2}	1.902 74		n^2_{O2}	1.913 01
	n^1_{O4}	1.944 79		n^1_{O4}	1.962 24
	n^2_{O4}	1.904 24		n^2_{O4}	1.904 08
	σ^*_{O2-Si3}	0.086 70		σ^*_{O2-C3}	0.078 58
	σ^*_{Si3-O4}	0.088 02		σ^*_{C3-O4}	0.073 36
TT	n^1_{O2}	1.941 99	TT	n^1_{O2}	1.951 56
	n^2_{O2}	1.911 94		n^2_{O2}	1.922 90
	n^1_{O4}	1.941 83		n^1_{O4}	1.951 56
	n^2_{O4}	1.911 71		n^2_{O4}	1.922 89
	σ^*_{O2-Si3}	0.060 21		σ^*_{O2-C3}	0.056 98
	σ^*_{Si3-O4}	0.059 86		σ^*_{C3-O4}	0.057 02

σ^*_{C3-O4} acceptor orbitals) in DMP resulted in an increase of 0.03% in the energy. This observation strongly suggests that the hyperconjugative interactions involving the antibonding orbitals play a more important role in DMP than in DMDMS in deciding conformational preferences. This conclusion is also in keeping with the observation that the energy difference between the $G^{\pm}G^{\mp}$ and $G^{\pm}T$ conformers in DMP is larger than in DMDMS.

It may also be noted from Table 4, that in the ground state $G^{\pm}G^{\mp}$structure, the energy difference, between the acceptor and donor orbitals in DMP and DMDMS (i.e., between the donor lone pair on oxygen and the acceptor antibonding C−O or Si−O orbital) are nearly the same. However, as noted earlier, the delocalization energies are smaller in DMDMS than in DMP. This point is also reinforced if we note that the off-diagonal Fock matrix element, which is a measure of the overlap, is smaller in DMMS than in DMP (Table 4). An examination of the electron occupancies in the NBOs of DMP also shows a consistent picture. It was mentioned earlier, that in the $G^{\pm}G^{\mp}$ conformer of DMDMS, the occupancies of the lone pair orbitals on O2 and O4 involved in hyperconjugation, was reduced by about 0.0438e relative to the orbitals on these oxygens, not involved in the delocalization. In DMP, the reduction in the occupancies of the corresponding orbitals is 0.0559e (Table 5), which is clearly larger and is indicative of the stronger hyperconjugative effects in DMP relative to DMDMS.

Dipole Moment. The dipole moment of the ground state conformer with $G^{\pm}G^{\mp}$ conformer in DMDMS was calculated to be 0.4 D, which is significantly less, compared with the $G^{\pm}T$ conformer with a dipole moment of 1.7 D. The net dipole

TABLE 6: Orbitals Deleted, Deletion Energies (Hartrees), Change in Energy (Hartrees and kcal/mol) for $G^{\pm}G^{\mp}$, $G^{\pm}T$, $G^{\pm}G^{\pm}$ and TT Conformers of DMDMS and DMP, with NBO Analysis Done at the HF/6-31++G Level.**

conformer	orbitals deleted	deletion energy (hartrees)	change in energy		relative change in deletion energy (%)
			hartrees	kcal/mol	
		DMDMS[a]			
$G^{\pm}G^{\mp}$	σ^*_{O2-Si3}	−597.167498828	0.056727	35.597	0.0095
	σ^*_{Si3-O4}	−597.167546127	0.056680	35.567	0.0095
	σ^*_{O2-Si3}	−597.111044190	0.113182	71.023	0.0190
	σ^*_{Si3-O4}				
GT	σ^*_{O2-Si3}	−597.176713375	0.045541	28.577	0.0080
	σ^*_{Si3-O4}	−597.168612186	0.053642	33.661	0.0090
	σ^*_{O2-Si3}	−597.122839936	0.099414	62.383	0.0170
	σ^*_{Si3-O4}				
$G^{\pm}G^{\pm}$	σ^*_{O2-Si3}	−597.176713375	0.045541	28.577	0.0076
	σ^*_{Si3-O4}	−597.168612186	0.053642	33.661	0.0090
	σ^*_{O2-Si3}	−597.109809987	0.111796	70.153	0.0187
	σ^*_{Si3-O4}				
TT	σ^*_{O2-Si3}	−597.172879818	0.045241	28.389	0.0076
	σ^*_{Si3-O4}	−597.172760644	0.045360	28.464	0.0076
	σ^*_{O2-Si3}	597.126874423	0.091247	57.258	0.0153
	σ^*_{Si3-O4}				
		DMP[b]			
$G^{\pm}G^{\mp}$	σ^*_{O2-C3}	−346.004917234	0.052305	32.822	0.015
	σ^*_{C3-O4}	−346.004913494	0.052308	32.824	0.015
	σ^*_{O2-C3}	−345.953163940	0.104058	65.297	0.030
	σ^*_{C3-O4}				
GT	σ^*_{O2-C3}	−346.009315687	0.042055	26.390	0.012
	σ^*_{C3-O4}	−346.000933298	0.050437	31.650	0.015
	σ^*_{O2-C3}	−345.959500236	0.091870	57.649	0.027
	σ^*_{C3-O4}				
$G^{\pm}G^{\pm}$	σ^*_{O2-C3}	−345.996541676	0.052453	32.915	0.015
	σ^*_{C3-O4}	−345.998766393	0.050228	31.519	0.015
	σ^*_{O2-C3}	−345.946757718	0.102237	64.155	0.030
	σ^*_{C3-O4}				
TT	σ^*_{O2-C3}	−346.000783003	0.042569	26.712	0.012
	σ^*_{C3-O4}	−346.000774735	0.042577	26.718	0.012
	σ^*_{O2-C3}	−345.958948929	0.084403	52.964	0.024
	σ^*_{C3-O4}				

[a] SCF energy (hartrees): $G^{\pm}G^{\mp}$, −597.2242419; $G^{\pm}T$, −597.2222703; $G^{\pm}G^{\pm}$, −597.2216060; TT, −597.218121137. [b] SCF energy (hartrees): $G^{\pm}G^{\mp}$, −346.0572218; $G^{\pm}T$, −346.0513704; $G^{\pm}G^{\pm}$, −346.04899448; TT, −346.043351946.

moment of DMDMS was calculated to be 0.93 D; a value that compares not too unfavorably with the experimental value of 1.3 D reported by Matsumura,[51] based on his measurements in benzene.

Conclusions

Matrix isolation infrared spectra of DMDMS in argon and nitrogen matrixes were recorded using an effusive source. Calculations performed at the B3LYP/6-31++G** level showed the ground state conformer to be one with a $G^{\pm}G^{\mp}$ structure, while the first two higher energy conformer had a $G^{\pm}T$ and $G^{\pm}G^{\pm}$ structures. Computed vibrational frequencies of the ground state conformer agreed well with experimentally observed values. NBO anlaysis revealed the operation of the anomeric interactions between lone pair oribitals in oxygen and σ^* orbital of Si−O, which stabilizes the gauche form of the molecule. A comparison of the NBO calculations for DMDMS and the corresponding carbon analogue, DMP, clearly reveals that the magnitude of the anomeric interaction is less in the Si compound than in DMP. This conclusion is in agreement with certain earlier reports that the anomeric interactions are indeed less in Si compounds than in corresponding C compounds.[52,53] However, the anomeric interactions in the silicon compounds are still large enough to generally retain the gauche−gauche conformer as the ground state, in the silicon systems that we have studied.

Acknowledgment. V.K. gratefully acknowledges the grant of a research fellowship from the Council of Scientific and Industrial Research (CSIR), India.

References and Notes

(1) Cossé−Barbi, A.; Jacques-Emile, D. *J. Am. Chem. Soc.* **1987**, *109*, 1503.
(2) Briggs, A. J.; Glenn, R.; Jones, P. G.; Kirby, A. J.; Ramaswamy, P. *J. Am. Chem. Soc.* **1984**, *106*, 6200.
(3) Taddei, F.; Kleinpeter, E. *J. Mol. Struct.* (*THEOCHEM*) **2004**, *683*, 29.
(4) Taddei, F.; Kleinpeter, E. *J. Mol. Struct.* (*THEOCHEM*) **2005**, *718*, 141.
(5) Cramer, C. J.; Truhler, D. G.; French, A. D. *Carbohydr. Res.* **1997**, *298*, 1.
(6) Salzner, U.; Schleyer, P. v. R. *J. Am. Chem. Soc.* **1993**, *115*, 10231.
(7) Senderowitz, H.; Fuchs, B. *J. Mol. Struct.* (*THEOCHEM*) **1997**, *395*−*396*, 123.
(8) Vilsmaier, E.; Dotzauer, M.; Wagemann, R.; Tetzlaff, C.; Fath, J.; Schlag, W-.R.; Bergsträβer, U. *Tetrahedron* **1995**, *51*, 11183.
(9) Cortés, F.; Tenorio, J.; Collera, O.; Cuevas, G. *J. Org. Chem.* **2001**, *66*, 2918.
(10) Sawanobori, M.; Sasanuma, Y.; Kaito, A. *Macromolecules* **2001**, *34*, 8321.
(11) Cuevas, G. *J. Am. Chem. Soc.* **2000**, *122*, 692.
(12) Sélambarom, T.; Carré, F.; Fruchier, A.; Roque, J. P.; Pavia, A. A. *Tetrahedron* **2002**, *58*, 4439.
(13) Nukada, T.; Bérces, A.; Whitfield, D. M. *Carbohydr. Res.* **2002**, *337*, 765.
(14) Nagumo, S.; Mizukami, M.; Akutsu, N.; Nishida, A.; Kawahara, N. *Tetrahedron Lett.* **1999**, *10*, 3209.
(15) Box, V. G. S. *J. Mol. Struct.* (*THEOCHEM*) **2001**, *569*, 167.
(16) Hernandez, S.; Ford, H., Jr.; Marquez, V. E. *Bioorg. Med. Chem.* **2002**, *10*, 2723.
(17) Tvaroška, I.; Carver, J. P. *Carbohydr. Res.* **1998**, *309*, 1.
(18) Cramer, C. J. *J. Mol. Struct.* (*THEOCHEM*) **1996**, *370*, 135.
(19) Bitzer, R. S.; Barbosa, A. G. H.; da Silva, C. O.; Nascimento, M. A. C. *Carbohydr. Res.* **2005**, *340*, 2171.
(20) Nukada, T.; Bérces, A.; Whitfield, D. M. *Carbohydr. Res.* **2002**, *337*, 765.
(21) Batchelor, R. J.; Green, D. F.; Johnston, B. D.; B. Patrick, O.; Pinto, B. M. *Carbohydr. Res.* **2001**, *330*, 421.
(22) Lii, J.-H.; Chen, K. H.; Allinger, N. L. *J. Comput. Chem.* **2003**, *24*, 1504.
(23) Lii, J.-H.; Chen, K.-H.; Durkin, K. A.; Allinger, N. L. *J. Comput. Chem.* **2003**, *24*, 1473.
(24) Tzou, D. L. M. *Solid State Nucl. Magn. Reson.* **2005**, *27*, 209.
(25) Balaban, T. S.; Eichhöfer, A.; Ghiviriga, I.; Hugo, H.; Wenzel, W. *J. Org. Chem.* **2003**, *68*, 5331.
(26) Vijgen, S.; Nauwelaerts, K.; Wang, J.; Aerschot, A. V.; Lagoja, I.; Herdewijn, P. *J. Org. Chem.* **2005**, *70*, 4591.
(27) Chiodini, L.; Malatesta, V.; Fusco, R.; Ranghino, G.; Scordamaglia, R.; Tosi, C. *J. Mol. Struct.* (*THEOCHEM*) **1986**, *138*, 51.
(28) Booth, H.; Dixon, J. M.; Khedhair, K. A. *Tetrahedron* **1992**, *48*, 6161.
(29) Venkatesan, V.; Sundararajan, K.; Sankaran, K.; Viswanathan, K. S. *Spectrochim. Acta. Part, A.* **2002**, *58*, 467.
(30) Venkatesan, V.; Sundararajan, K.; Viswanathan, K. S. *J. Phys. Chem. A.* **2002**, *106*, 7707.
(31) Venkatesan, V.; Sundararajan, K.; Viswanathan, K. S. *Spectrochim. Acta Part, A.* **2003**, *59*, 1497.
(32) Kavitha, V.; Sundararajan, K.; Viswanathan, K. S. *J. Phys. Chem. A.* **2005**, *109*, 9259.
(33) Kavitha, V.; Sankaran, K.; Viswanathan, K. S. *J. Mol. Struct.* **2006**, *791*, 165.
(34) Wider, D. C.; Moore, J. H.; Tossell, J. A. *Chem. Phys. Lett.* **1994**, *222*, l.
(35) Tajima, S.; Sekiguchi, O.; Watanabe, Y.; Nakajima, S.; Takahashi, Y. *J. Mass Spectrom.* **2001**, *36*, 816.
(36) Sutherland, D. G.; Bancroft, G. M.; Tan, K. H. *J. Chem. Phys.* **1992**, *97*, 7918.
(37) Maier, G.; Glatthaar, J. *Eur. J. Org. Chem.* **2003**, 3350.
(38) Ignatyev, I. S.; Montejo, M.; Partal Ureña, F.; Sundius, T.; López González, J. J. *Vib. Spectrosc.* **2006**, *40*, 1.
(39) George, L.; Sankaran, K.; Viswanathan, K. S.; Mathews, C. K. *Appl. Spectrosc.* **1994**, *48*, 7.
(40) Vidya, V.; Sankaran, K.; Viswanathan, K. S. *Chem. Phys. Lett.* **1996**, *258*, 113.
(41) George, L.; Viswanathan, K. S.; Singh, S. *J. Phys. Chem. A.* **1997**, *101*, 2459.
(42) Frisch, M. J.; Trucks, G. W.; Schlegel, H. B.; Scuseria, G. E.; Robb, M. A.; Cheeseman, J. R.; Zakrzewski, V. G.; Montgomery, J. A., Jr.; Stratmann, R. E.; Burant, J. C.; Dapprich, S.; Millam, J. M.; Daniels, A. D.; Kudin, K. N.; Strain, M. C.; Farkas, O.; Tomasi, J.; Barone, V.; Cossi, M.; Cammi, R.; Mennucci, B.; Pomelli, C.; Adamo, C.; Clifford, S.; Ochterski, J.; Petersson, G. A.; Ayala, P. Y.; Cui, Q.; Morokuma, K.; Malick, D. K.; Rabuck, A. D.; Raghavachari, K.; Foresman, J. B.; Cioslowski, J.; Ortiz, J. V.; Baboul, A. G.; Stefanov, B. B.; Liu, G.; Liashenko, A.; Piskorz, P.; Komaromi, I.; Gomperts, R.; Martin, R. L.; Fox, D. J.; Keith, T.; Al-Laham, M. A.; Peng, C. Y.; Nanayakkara, A.; Challacombe, M.; Gill, P. M. W.; Johnson, B.; Chen, W.; Wong, M. W.; Andres, J. L.; Gonzalez, C.; Head-Gordon, M.; Replogle, E. S.; Pople, J. A. *Gaussian 98*, Revision A.9; Gaussian Inc.: Pittsburgh PA, 1998.
(43) The spectra were simulated using SYNSPEC made available by K. Irikura: SYNSPEC; National Institute of Standards and Technology: Gaithesburg, MD, 1995.
(44) Moon, S.; Kwon, Y.; Lee, J.; Choo, J. *J. Phys. Chem. A.* **2001**, *105*, 3221.
(45) Sproviero, E. M.; Burton, G. *J. Phys. Chem. A.* **2003**, *107*, 5544.
(46) Roohi, H.; Ebrahimi, A. *J. Mol. Struct.* (*THEOCHEM*) **2005**, *726*, 139.
(47) Wang, W.; Pu, X.; Zheng, W.; Wong, N-B.; Tian, A. *Chem. Phys. Lett.* **2003**, *370*, 147.
(48) Gupta, N.; Shah, K. Kr.; Garg, R. J. *Org. Chem.* **2006**, *71*, 1344.
(49) Benassi, R.; Bertarini, C.; Taddei, F. *J. Mol. Struct.* (*THEOCHEM*) **1995**, *339*, 103.
(50) Reva, I. D.; Stepanian, S. G.; Adamowicz, L.; Fausto, R. *Chem. Phys. Lett.* **2003**, *374*, 631.
(51) Matsumura, K. *Bull. Chem. Soc. Jpn.* **1962**, *35*, 801.
(52) Pavan Kumar, P. N. V; Wang, D. X.; Lam, B.; Albright, T. A.; Jemmis, E. D. *J. Mol. Struct.* **1989**, *194*, 183.
(53) Apeloig, Y.; Stanger, A. *J. Organomet. Chem.* **1988**, *346*, 305.